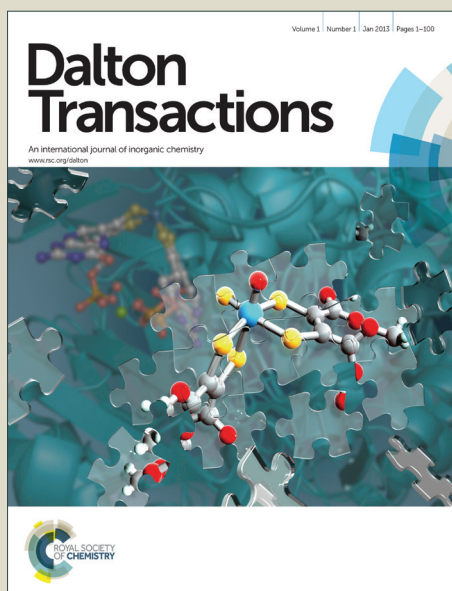


# Dalton Transactions

Accepted Manuscript



This is an *Accepted Manuscript*, which has been through the Royal Society of Chemistry peer review process and has been accepted for publication.

*Accepted Manuscripts* are published online shortly after acceptance, before technical editing, formatting and proof reading. Using this free service, authors can make their results available to the community, in citable form, before we publish the edited article. We will replace this *Accepted Manuscript* with the edited and formatted *Advance Article* as soon as it is available.

You can find more information about *Accepted Manuscripts* in the [Information for Authors](#).

Please note that technical editing may introduce minor changes to the text and/or graphics, which may alter content. The journal's standard [Terms & Conditions](#) and the [Ethical guidelines](#) still apply. In no event shall the Royal Society of Chemistry be held responsible for any errors or omissions in this *Accepted Manuscript* or any consequences arising from the use of any information it contains.

Cite this: DOI: 10.1039/c0xx00000x

www.rsc.org/xxxxxx

ARTICLE TYPE

## Cytochrome P450-Catalyzed Dealkylation of Atrazine by *Rhodococcus* sp. strain NI86/21 Involves Hydrogen Atom Transfer rather than Single Electron Transfer

Armin H. Meyer<sup>a</sup>, Agnieszka Dybala-Defratyka<sup>b,d</sup>, Peter J. Alaimo<sup>c</sup>, Inacrist Geronimo<sup>b</sup>, Ariana D. Sanchez<sup>c</sup>, Christopher J. Cramer<sup>d</sup> and Martin Elsner<sup>a\*</sup>

Received (in XXX, XXX) Xth XXXXXXXXX 20XX, Accepted Xth XXXXXXXXX 20XX

DOI: 10.1039/b000000x

**ABSTRACT:** Cytochrome P450 enzymes are responsible for a multitude of natural transformation reactions. For oxidative N-dealkylation, single electron (SET) and hydrogen atom abstraction (HAT) have been debated as underlying mechanisms. Combined evidence from (i) product distribution and (ii) isotope effects indicate that HAT, rather than SET, initiates N-dealkylation of atrazine to desethyl- and desisopropylatrazine by the microorganism *Rhodococcus* sp. strain NI86/21. (i) Product analysis revealed a non-selective oxidation at both the  $\alpha$ C and  $\beta$ C-atom of the alkyl chain, which is expected for a radical reaction, but not SET. (ii) Normal  $^{13}\text{C}$  and  $^{15}\text{N}$  as well as pronounced  $^2\text{H}$  isotope effects ( $\epsilon_{\text{carbon}}$ :  $-4.0\text{‰} \pm 0.2\text{‰}$ ;  $\epsilon_{\text{nitrogen}}$ :  $-1.4\text{‰} \pm 0.3\text{‰}$ ,  $\text{KIE}_{\text{H}}$ :  $3.6 \pm 0.8$ ) agree qualitatively with calculated values for HAT, whereas inverse  $^{13}\text{C}$  and  $^{15}\text{N}$  isotope effects are predicted for SET. Analogous results are observed with the Fe(IV)=O model system [5,10,15,20-tetrakis(pentafluoro-phenyl)porphyrin-iron(III)-chloride + NaIO<sub>4</sub>], but not with permanganate. These results emphasize the relevance of the HAT mechanism for N-dealkylation by P450.



Cite this: DOI: 10.1039/c0xx00000x

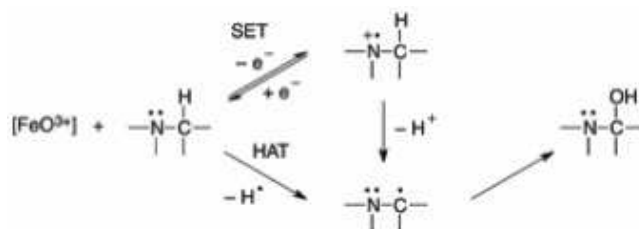
www.rsc.org/xxxxxx

ARTICLE TYPE

## INTRODUCTION

Cytochrome P450 (P450) enzymes are known to catalyze a multitude of natural transformation reactions<sup>1, 2</sup>. They are involved in human metabolism of steroids, drugs and xenobiotics<sup>3</sup> and in bioremediation of environmental contaminants by fungi and bacteria<sup>4</sup>. The importance of understanding these natural reactions, and of engineering improved P450-based catalysts for biotechnical and pharmaceutical industries,<sup>5,6, 7</sup> has motivated much fundamental research on the catalytic mechanism which determines reactivity, specificity and selectivity.<sup>8, 9, 10, 11</sup>. While evidence points to hydrogen atom transfer (HAT) for selective hydroxylation of hydrocarbons<sup>12</sup>, the underlying biochemical reaction mechanism leading to N-dealkylation of N-bound alkyl groups such as in alkaloids<sup>13</sup>, alkylanilines<sup>14</sup>, triazines and phenylurea herbicides<sup>15</sup>, has been contested<sup>16</sup>. For decades two possible reaction mechanisms have been hypothesized<sup>17-24</sup> (Scheme 1). The first mechanism involves a single-electron-transfer (SET) in the initial step, where an electron from the N-atom is transferred to the high valent iron-oxygen center (Fe(IV)=O, or FeO<sup>3+</sup>) of the cytochrome P450.

### Scheme 1. Mechanisms hypothesized for oxidative dealkylation catalysed by cytochrome P-450 monooxygenase: single electron transfer (SET); hydrogen atom abstraction (HAT).



The resulting aminium cation radical releases H<sup>+</sup> from an adjacent C-H bond. The second mechanism – a hydrogen atom abstraction (HAT) – starts directly with homolytic cleavage of the C-H bond adjacent to the heteroatom. Both pathways produce the same relatively unstable 1,1-aminoalcohol (Scheme 1) which subsequently eliminates to form an aldehyde or ketone and further decays to the N-dealkylated product<sup>25</sup>.

The strongest evidence for SET so far has been given by an inverse Linear Free Energy Relationship between the rate of N-dealkylation of different N,N-dimethylanilines and the Hammett parameter  $\sigma$ <sup>26, 27</sup>. Further support for this mechanism is provided by small intermolecular and intramolecular kinetic hydrogen isotope effects (<sup>1</sup>k/<sup>2</sup>k = 1-2) observed during amine dealkylation<sup>14, 20</sup>, which indicate that the C-H bond is not broken in the initial

step<sup>28</sup>. In contrast, large intramolecular hydrogen isotope effects (<sup>2</sup>k/<sup>1</sup>k > 7) observed during the oxidation of amides provided evidence that the C-H bond was initially cleaved<sup>18, 21, 29</sup>. Further, N-demethylation of dimethylanilines by P450 enzymes showed similar hydrogen isotope effect profiles as for H-atom abstraction by tert-butoxy radicals<sup>17, 30</sup> suggesting a HAT mechanism as the initial step. However, hydrogen isotope effects are often masked by rate determining steps other than the C-H cleavage and may show a rather large variability even in the absence of masking<sup>31</sup> so that they need to be discussed critically for their ability to provide conclusive mechanistic insight<sup>23, 32</sup>. Therefore, although much research has been dedicated to confirming or discarding these alternative mechanisms, the nature of the initial step remains subject to debate<sup>19, 33, 34</sup>.

The objective of this study was to elucidate for the first time the transformation mechanism for oxidative dealkylation of the triazine herbicides atrazine and simazine, in particular whether SET or HAT is the initial step in the cytochrome P450 catalyzed N-dealkylation.

We used the bacterial strain *Rhodococcus* sp. strain NI86/21 as model organism closely mimicking natural conditions. It contains a single cytochrome P450 monooxygenase system (member of the CYP 116 family), as conclusively demonstrated by atrazine-negative mutants, which were re-activated by transfer of the specific cytochrome P-450 gene.<sup>35, 36</sup> This organism is known to catalyze the oxidation of atrazine to DEA and DIP with hydroxyisopropyl atrazine as an additional identified product (i.e., with -OH in the  $\beta$ -position of the isopropyl group, see Fig. 1)<sup>35, 36</sup>. To compare our observations to a reference reaction for Fe(IV)=O, we investigated oxidative degradation in the metalloporphyrin system 5,10,15,20-tetrakis(pentafluorophenyl)porphyrin-iron(III)-chloride (FeP) where the iron(III) porphyrin becomes activated by iodate through peroxide shunt<sup>19, 33, 34</sup> to mimic the reactivity of FeO<sup>3+</sup> in P450 monooxygenases<sup>37</sup>.

Finally, we included permanganate as an additional reactant for selective oxidation only in the  $\alpha$ -position. Studies on the oxidation of ethers and primary amines have established (i) a high selectivity for C-H bonds with the lowest dissociation energy and (ii) a direct attack at the C-H bond<sup>38-40</sup>, where the activated complex at pH 7 in an aqueous solution was hypothesized to be comparable to either HAT<sup>38, 41</sup> or to an associative hydride transfer where a hydroxide displaces the hydride when it is being abstracted by the oxygen of Mn-O<sup>40</sup>.

In our approach we pursued two lines of evidence that have not been systematically combined for this question previously. (i) Metabolites were identified and quantified during atrazine and simazine degradation, with a particular focus on the molecular position of the -OH group substitution in hydroxylated intermediates. Putative intermediates were identified by LC-MS/MS (liquid chromatography coupled to tandem mass spectrometry). In addition an authentic standard of the putative

metabolite with a hydroxyl group in  $\beta$ -position of the ethyl-group was specifically synthesized (2-((4-chloro-6-(isopropylamino)-1,3,5-triazine-2-yl)amino)ethanol). (ii) Carbon and nitrogen isotope effects were measured in atrazine and simazine, with gas chromatography – isotope ratio mass spectrometry (GC-IRMS). This analysis gives the average of isotope effects over all positions in the triazine substrate. While such average values are smaller than position-specific isotope effects at reacting bonds, they have the advantage that they can be measured with high precision. GC-IRMS analysis of single data points has typical uncertainties ( $2\sigma$ ) of 0.5‰ ( $^{13}\text{C}/^{12}\text{C}$ ) and 1‰ ( $^{15}\text{N}/^{14}\text{N}$ ).<sup>47</sup> Since kinetic isotope effects are determined by regression through numerous data points, they are typically determined with a precision (95% confidence intervals) of a few tenths of one per mille.

Further, hydrogen isotope effects in the side chain were determined with deuterated simazine as substrate. At the same time, isotope effects for SET and HAT were computed theoretically at the SMD/M06-2X/6-31++G(d,p) level of theory. The usefulness of density functional theory calculations for predicting isotope effects is well established from recent publications<sup>42,43</sup>.

Our approach was based on two hypotheses. (i) *Selectivity of product formation*. Oxidation of the nitrogen atom (SET) is expected to produce C-OH groups solely in the  $\alpha$ -position, because this C-H bond is cleaved as a result of the adjacent aminium radical cation. In contrast, the radical reaction (HAT) is potentially non-specific and may lead to products with C-OH groups also in the  $\beta$ -positions. (ii) *Evidence from isotope effects*. Kinetic isotope effects in the parent compound have the virtue that they only depend on the first step of a reaction (i.e., HAT vs. SET) and are independent of further reactions of metabolites. It was, therefore, our objective to investigate whether also isotope effects can be indicative of the prevailing transformation mechanism as brought forward in previous studies<sup>44-47</sup>. For SET an inverse N isotope effect (depletion of the  $^{15}\text{N}$ -isotopologue in the residual substance pool) was observed by Skarpeli-Liati et al.<sup>48</sup> in oxidation of substituted anilines by manganese oxide. Using computational calculations, we aimed to investigate whether a similar inverse isotope effect is predicted for atrazine, and whether the opposite pattern - a normal secondary N-isotope effect (enrichment of the  $^{15}\text{N}$ -isotopologue in the residual substance pool) - would be expected for HAT.

## MATERIAL AND METHODS

**Chemicals.** A complete list of the chemicals used and their providers is provided in the Supporting Information (SI).

**Bacterial strain and cultivation media.** *Rhodococcus* sp. strain NI86/21 was purchased from the National Collection of Agricultural and Industrial Microorganisms (Budapest, Hungary). The strain was grown in autoclaved nutrient broth (15g/L, pH: 6.9) (Roth, Karlsruhe, Germany) containing either atrazine (90  $\mu\text{M}$ ) or simazine (60  $\mu\text{M}$ ). For the degradation experiment 100  $\mu\text{L}$  of cell suspension (OD<sub>580nm</sub>: 1.2 – 1.5) was transferred to about 400 mL fresh nutrient broth solution containing atrazine, simazine or 1:1 mixture of simazine and simazined10. Experiments were carried out in triplicates at 21 °C. Control experiments, carried out

in the absence of the bacterial strain, did not show any degradation of simazine or atrazine (results not shown).

### Oxidative degradation with potassium permanganate.

Triplicate experiments were carried out in a phosphate-buffered (10 mM, pH: 7.1) aqueous (deionized water) solution (500 mL) at 21 °C in the dark. Concentrations of atrazine or simazine solutions were between 60  $\mu\text{M}$  and 80  $\mu\text{M}$ . The concentration of the oxidant  $\text{KMnO}_4$  was 0.1 M. To demonstrate selective oxidation of the ethyl group of atrazine, we conducted a negative control experiment with propazine (2,4-bis(isopropylamino)-6-chloro-1,3,5-triazine; CAS: 139-40-2) (13  $\mu\text{M}$ ) under the same reaction conditions in which degradation was not observed (see SI, Figure S1).

**Oxidative degradation with a metalloporphyrin system.**  $\text{NaO}_4$  (13.6 mg) and 5,10,15,20-tetrakis(pentafluoro-phenyl)porphyrin-iron(III)-chloride (5 mg) were added to 22.5 mL acetonitrile and dispersed in an ultrasonic bath for 2 min. Addition of 2.5 mL of an atrazine stock solution (100 mg/L; dissolved in acetonitrile) gave an initial molar ratio of porphyrin / oxidant / substrate of 10/56/1. The experiment was performed at 60 °C in the dark and was carried out in eight independent batches which were sacrificed at different time points.

**Synthesis of the standard 2-((4-chloro-6-(isopropylamino)-1,3,5-triazine-2-yl)amino)ethanol.** All materials were obtained from commercial sources and were used without further purification. The synthesis was conducted according to modified literature procedures<sup>49,50</sup>, as specified below and further in the SI.

*2-((4,6-dichloro-1,3,5-triazin-2-yl)amino)ethanol* (**2**, intermediate). A 500 mL round bottom flask was charged with cyanuric chloride (18.4 g; 100 mmol), acetone (100 mL) and water (100 mL). The resulting mixture was cooled (0 °C), and then with rapid stirring a biphasic mixture of ethanolamine (6.3 mL; 105 mmol) and diethyl ether (20 mL) was added dropwise over 5 min. Subsequently, a solution of  $\text{NaHCO}_3$  (16.8 g, 200 mmol) in water (150 mL) was added over 10 min. The mixture was stirred at 0 °C for 1h, and then allowed to warm to room temperature and stirred overnight. The reaction was partitioned between ethyl acetate (300 mL) and water (200 mL) and the aqueous layer was extracted with ethyl acetate (4 x 200 mL). The combined organic layers were washed with saturated  $\text{NaHCO}_3$  (200 mL), brine (200 mL), and dried over anhydrous  $\text{MgSO}_4$ . The solution was filtered, the volatile materials of the filtrate were evaporated under reduced pressure, and the remaining residue was dried in vacuo (0.1 torr for 16 h) to give **2** (Figure S2) as a white crystalline solid (13.6 g; 65.2 mmol; 65.2 %). Compound **2** was used without further purification.  $^1\text{H}$  NMR (400 MHz,  $(\text{CD}_3)_2\text{SO}$ ):  $\delta$  9.10 (t, J=6 Hz, 1H), 4.50 (br s, 1H), 3.50 (t, J=6 Hz, 2H), 3.36 (t, J=6 Hz, 2H).  $^{13}\text{C}$  NMR (100 MHz,  $(\text{CD}_3)_2\text{SO}$ ):  $\delta$  169.3, 168.4, 165.4, 58.7, 43.4. Lit.<sup>49</sup>  $^{13}\text{C}$  NMR (150 MHz,  $(\text{CD}_3)_2\text{SO}$ ):  $\delta$  170.0, 169.1, 166.1, 59.4, 44.1.

*2-((4-chloro-6-(isopropylamino)-1,3,5-triazin-2-yl)amino) ethanol* (**3**, target compound). A 500 mL round bottom flask was charged with compound **2** (3.6 g; 17.2 mmol), absolute ethanol (200 mL),  $\text{Na}_2\text{CO}_3$  (4.01 g; 37.8 mmol), and isopropylamine (2.7 mL; 33.0 mmol). The flask was fitted with a condenser, and heated to 35 °C for 16 h. The mixture was cooled to room temperature, and

Cite this: DOI: 10.1039/c0xx00000x

www.rsc.org/xxxxxx

ARTICLE TYPE

partitioned between ethyl acetate (200 mL) and water (200 mL). The aqueous layer was extracted with ethyl acetate (3 x 150 mL), and the combined organic layers were washed with brine (200 mL) and dried over anhydrous MgSO<sub>4</sub>. The solution was filtered, volatile materials of the filtrate were evaporated under reduced pressure, and the residue was dried in vacuo (0.1 torr for 16 h) to give crude product **3** as a white crystalline solid (3.74 g; 16.1 mmol; 93.5 %). A portion of crude product **3** (500 mg) was purified by column chromatography (SiO<sub>2</sub>; 95:5 CH<sub>2</sub>Cl<sub>2</sub>:MeOH) to give 431 mg of a white solid that showed only 1 spot by TLC, but appeared (by <sup>13</sup>C NMR) to be an inseparable mixture of isomers or tautomers. TLC (SiO<sub>2</sub>, 95:5 CH<sub>2</sub>Cl<sub>2</sub>:MeOH): R<sub>f</sub> = 0.29 (254 nm or KMnO<sub>4</sub>). <sup>1</sup>H NMR (400 MHz, (CD<sub>3</sub>)<sub>2</sub>SO): δ 7.76-7.55 (m, <sup>2</sup>H), 4.71-4.66 (m, 1H), 4.06-3.96 (m, 1H), 3.52-3.43 (m, 2H), 3.33-3.25 (m, 2H), 1.13 (m, 6H). Lit.<sup>49</sup> <sup>1</sup>H NMR (600 MHz, (CD<sub>3</sub>)<sub>2</sub>SO): δ 7.76-7.69 (m, 1H), 7.67-7.56 (m, 1H), 4.70-4.66 (m, 1H), 4.04-3.94 (m, 1 H), 3.50-3.42 (m, 2H), 3.31-3.24 (m, 2H), 1.11 (d, J=6.5 Hz, 3H), 1.09 (d, J=6.5, 3H). <sup>13</sup>C NMR (100 MHz, (CD<sub>3</sub>)<sub>2</sub>SO; possibly a mixture of isomers or tautomers): δ 168.0, 167.5, 165.6, 165.4, 165.0, 164.5, 164.3, 164.0, 59.3, 59.2, 42.9, 42.7, 41.9, 41.6, 22.3, 21.9. Lit.<sup>49</sup> <sup>13</sup>C NMR (150 MHz, (CD<sub>3</sub>)<sub>2</sub>SO): δ 168.6, 166.5, 165.4, 60.28, 44.0, 43.0, 23.0.

**Quantification and identification of atrazine, simazine and its metabolites.** For concentration measurements of desethylatrazine, desisopropylatrazine (= desethylsimazine) and hydroxyatrazine, 150 µL samples were taken, of which 20 µL were analyzed using a Shimadzu LC-10A series HPLC system using an ODS column 30 (Ultracarb 5µM, 150 x 4.6 mm, Phenomenex, Aschaffenburg). A more detailed description of analytical conditions is provided in the SI.

**Identification of further metabolites.** For the identification of unknown peaks 150 µL sample were frozen until analysis. 10 µL of the sample were analyzed using an Agilent HP 1200 HPLC system coupled to a Q-Trap MS/MS system (Applied Biosystems, Toronto, Canada). Mass spectrometry was carried out in the Enhanced Product Ion scan mode. Ionisation was accomplished by electrospray ionization (ESI) in the positive ion mode, with an ion spray voltage of 4600 V. Declustering potential (DP) was 46 V, entrance potential (EP) 4.5 V, collision energy (CE) 23 eV, and collision cell exit potential was 4 eV. Nitrogen was used as a curtain gas, collision gas, turbo gas and nebulizer gas. The temperature of the turbo gas was 400 °C. Further information about separation conditions is given in the SI.

**Carbon and nitrogen isotope analysis.** Samples for compound-specific isotope analysis of atrazine or simazine (15 mL – 200 mL) were extracted with 5-10 mL dichloromethane, which was

subsequently evaporated at room temperature under a hood. Extracts of the permanganate experiment were additionally filtered through glass wool. The remaining residues were redissolved in ethyl acetate to give atrazine and simazine concentrations of about 900 µM. Tests with standards showed no significant fractionation during the preparation steps. Each sample was analysed in duplicate. Two to four microliters of the extracts were injected with a GC Pal autosampler (CTC, Zwingen, Switzerland) onto a GC-C-IRMS system consisting of a TRACE GC Ultra gas chromatograph, a GC-III combustion interface and a Finnigan MAT253 IRMS (all Thermo Fisher Scientific, Milan, Germany). The injector was operated for 1 min in splitless and then in split mode (1:10), at 250°C with a column flow of 1.4 mL min<sup>-1</sup>. A DB-5 column (60 m x 0.25 mm; 1 µm film; J&W Scientific, Folsom; CA, USA) was used with a GC oven program of 140 °C (hold: 1 min), ramp 18 °C/min to 155 °C, ramp 2 °C/min to 240 °C, ramp 30 °C/min to 260 °C (hold: 5 min). For carbon isotope analysis analytes were combusted to CO<sub>2</sub> in a GC IsoLink oven (Thermo Fisher Scientific, Bremen, Germany) at 1050°C<sup>51</sup>. The analytical uncertainty was ± 0.7 ‰<sup>51</sup>. For N isotope analysis, analytes were converted to N<sub>2</sub> using the setup described in Hartenbach et al.<sup>52</sup>. The δ<sup>15</sup>N- and δ<sup>13</sup>C-values are reported in per mille relative to Vienna PeeDee Belemnite (V-PDB) and air respectively:

$$\delta^{13}\text{C} = \left[ \left( \frac{^{13}\text{C}/^{12}\text{C}_{\text{Sample}}}{^{13}\text{C}/^{12}\text{C}_{\text{Standard}}} - 1 \right) \right] \cdot 1000 \quad (1)$$

$$\delta^{15}\text{N} = \left[ \left( \frac{^{15}\text{N}/^{14}\text{N}_{\text{Sample}}}{^{15}\text{N}/^{14}\text{N}_{\text{Standard}}} - 1 \right) \right] \cdot 1000 \quad (2)$$

CO<sub>2</sub> and N<sub>2</sub> monitoring gases were calibrated against international reference materials RM 8562, RM 8563, RM 8564 (for CO<sub>2</sub>) and NSVEC (for N<sub>2</sub>)<sup>53</sup>.

**Evaluation of stable isotope fractionation.** Isotope enrichment factors for carbon and nitrogen were determined as the slope of a linear regression according to the Rayleigh-equation:

$$\ln \frac{R_t}{R_0} = \ln \left( \frac{1 + \delta^h E_t}{1 + \delta^h E_0} \right) = \varepsilon \cdot \ln f \quad (3)$$

in which R<sub>t</sub> and R<sub>0</sub> are the compound-specific isotope ratios of heavy versus light isotopes at a given time and at the beginning of the reaction. δ<sub>h</sub>E<sub>t</sub> and δ<sub>h</sub>E<sub>0</sub> are the isotopic signatures of the compound for the element E at times t and zero, respectively, while C<sub>t</sub>/C<sub>0</sub> is the fraction f of the remaining compound. In these experiments, the enrichment factor ε is a measure for the isotopic enrichment as average over all positions in a molecule according to<sup>54</sup>

$$\varepsilon \approx \left( \frac{1}{KIE_{\text{average}}} - 1 \right) \quad (4)$$

ε has a negative value for normal kinetic isotope effects and is

322 positive for inverse isotope effects.

323 Whereas the carbon and nitrogen GC-IRMS analysis was  
324 performed at natural isotopic abundance, deuterium-labelled  
325 simazine-*d*<sub>10</sub> (2,4-bis(pentadeuteroethylamino)-6-chloro-1,3,5-  
326 triazine) was used and analyzed by LC-MS/MS to determine  
327 position-specific hydrogen isotope effects in the ethyl side chain of  
328 simazine. From ratios  $R_0$  and  $R_t$  of simazine and simazine-*d*<sub>10</sub>  
329 during biodegradation at time 0 and  $t$ , a position-specific  $\epsilon_H$  was  
330 evaluated according to Hunkeler et al.<sup>55</sup>

$$332 \ln\left(\frac{R_t}{R_0}\right) = \frac{1}{\epsilon_H} \cdot \ln\left[\left(\frac{1+R_0}{1+R_t}\right) \cdot f\right] \quad (5)$$

333 with

$$334 \epsilon_H \approx \left(\frac{1}{KIE_{H, \text{ethyl side chain}}} - 1\right) \quad (6)$$

335  
336 Since  $\epsilon_H$  is a position-specific value, it was assumed to be  
337 representative also of the ethyl side chain in atrazine.

338  
339 **Dual element isotope plots.** To compare isotope effects of two  
340 elements simultaneously, measured isotope values, e.g.  $\delta^{13}\text{C}$  and  
341  $\delta^{15}\text{N}$ , were plotted against each other to give the slope

$$343 \Lambda = \frac{\Delta\delta^{15}\text{N}}{\Delta\delta^{13}\text{C}} \approx \frac{\epsilon_{\text{average, nitrogen}}}{\epsilon_{\text{average, carbon}}} \quad (7)$$

344  
345 Different slopes  $\Lambda$  in these dual element isotope plots correspond  
346 to different combinations of isotope effects  $KIE_{\text{average}}$  (see eq. 4)  
347 reflecting different underlying mechanisms<sup>56-60</sup>. Such dual  
348 element isotope representations have the advantage that their  
349 slopes tend to be insensitive towards masking<sup>61, 62</sup>. Observable  
350 (i.e., apparent) kinetic isotope effects (A)KIE may decrease  
351 dramatically in the presence of additional rate-limiting steps (e.g.,  
352 transport, substrate binding). In contrast, the slope (i.e., their ratio)  
353 remains more constant, because KIE of both elements typically  
354 decrease in equal proportion (provided that the additional steps do  
355 not show isotope effects themselves)<sup>56</sup>.

356 **Computational methods.** All molecular species were optimized  
357 at the density functional level of theory (DFT) employing the  
358 M06-2X hybrid meta-generalized-gradient functional<sup>63, 64</sup> and the  
359 6-31++G(d,p) basis set (restricted to 5 spherical d functions),<sup>65, 66</sup>  
360 during optimization, aqueous solvation effects were included  
361 using the SMD implicit solvation model<sup>67</sup>. The natures of all  
362 stationary points were confirmed by computation of analytical  
363 vibrational frequencies (3n - 6 real vibrations in the case of  
364 reactants and one imaginary frequency corresponding to the  
365 desired reaction coordinate in the case of transition-state  
366 structures). Open shell species were treated using unrestricted  
367 Kohn-Sham DFT. All calculations were performed in the  
368 Gaussian09 package<sup>68</sup>. In order to probe the SET mechanism,  
369 neutral and 1e oxidized forms of atrazine were used. <sup>15</sup>N and <sup>13</sup>C  
370 kinetic isotope effects were calculated according to the previously  
371 described approach of Skarpeli-Liati et al.<sup>48</sup> which followed with

372 slight modification the method of Kavner et al.<sup>69</sup> Driving forces  
373 were computed for a redox potential of atrazine of 0.800 V, which  
374 has been estimated from experiment to be a lower limit (Michael  
375 Sander, personal communication). We also predicted SET isotope  
376 effects for a potential of 0.678 V (the value computed at the M06-  
377 2X/6-311+G(2df,2p) level)<sup>70, 71</sup> and for higher values of 0.900 and  
378 1.000 V. The sensitivity of the predicted isotope effects over a 0.2  
379 eV range in driving force did not exceed 0.3%. Typical values of  
380 the reorganization energy  $\lambda$  were explored (100, 200, 300, 400  
381 kJ/mol); for a total driving force of 0.2 eV, the predicted KIEs  
382 varied by no more than 0.5% over the full  $\lambda$  range. The reported  
383 isotopic fractionation data were calculated for 300 kJ/mol.

384 We note here that our approach for computing KIEs for SET,  
385 allows for the prediction of kinetic isotope effects on electron  
386 transfer reactions within a semiclassical regime without  
387 consideration of isotope-sensitive electron tunneling probabilities,  
388 for which a more complete quantum mechanical approach would  
389 be required. Such an approach, pioneered by Jortner and co-  
390 workers<sup>72, 73</sup>, and used more recently by Roth et al.<sup>74</sup>, adopts a  
391 formalism to describe differential contributions from high-  
392 frequency modes that exceed the available thermal energy.  
393 However, application of the theory requires assumptions of  
394 limited utility for our purposes here. First, the theory assumes that  
395 the change in a single normal mode dominates the differential  
396 tunneling for electron-transfer, but for a molecule the size of  
397 atrazine in which the radical cation has delocalized character, the  
398 selection of a dominant mode is far from straightforward. In  
399 addition, the model of Jortner and co-workers depends on  
400 distortions from equilibrium bond lengths in the reactant and  
401 product states and, as reported for <sup>18</sup>O KIEs by Roth et al. for  
402 electron transfer to molecular oxygen (<sup>74</sup> Table 5), the magnitude  
403 of the calculated KIE is quite sensitive to the value of this  
404 distortion. However, the smaller the difference in bond lengths,  
405 the smaller the predicted influence on isotope effect. Again, in the  
406 case of a system more complex than diatomic O<sub>2</sub>, many bond  
407 lengths change and particularly in the case of atrazine, they  
408 change by rather small margins (at most 0.05 Å). Based on these  
409 observations, we consider it unlikely that consideration of  
410 differential tunneling effects could elevate the magnitudes of our  
411 predicted ET KIEs to be close to the measured values, as  
412 presented below.

413 Position-specific isotope effects for the HAT mechanism were  
414 obtained from the complete Bigeleisen equation<sup>75</sup> using the  
415 ISOEFF program<sup>76</sup> at 300 K for the transition from a reactant  
416 complex (a neutral atrazine molecule plus an accompanying  
417 perhydroxyl radical) to the corresponding HAT transition-state  
418 structure. Tunneling contributions were included using the  
419 method of Skodje et al.<sup>77</sup>. The calculations for  $\beta$ -oxidation were  
420 performed in the following way. The abstraction of all possible  
421 hydrogen atoms was taken into account at both sites of the  
422 atrazine molecule. This resulted in seven and five different  
423 pathways in the case of isopropyl and ethyl side chain,  
424 respectively. Then, all results (free energies, enthalpies, imaginary  
425 frequencies as well as position specific isotope effects) were  
426 averaged over all these obtained pathways. Coordinates of all  
427 fully optimized species are available in the SI.

## 428 RESULTS AND DISCUSSION

Cite this: DOI: 10.1039/c0xx00000x

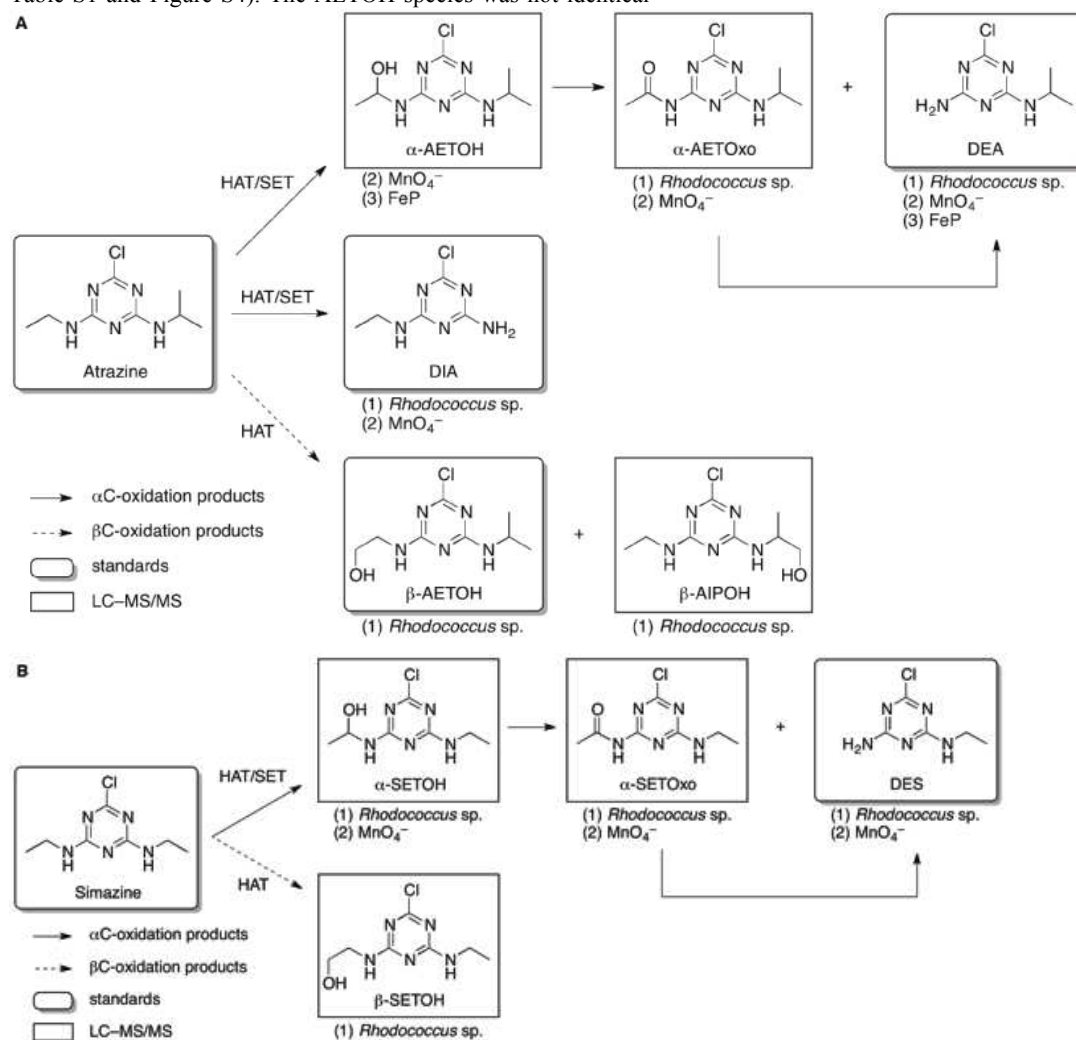
www.rsc.org/xxxxxx

ARTICLE TYPE

429 **(i) Insight from product formation.** Structures of putative and  
430 confirmed transformation products are summarized in Figure 1.  
431 Their identification and the corresponding pathway  
432 characterization were based on product analysis as laid out in the  
433 discussion of the following experiments.

434 *Degradation products in oxidation of atrazine with  $MnO_4^-$ .* The  
435 main transformation products from the oxidation of atrazine by  
436 permanganate were DEA and DIA in a proportion of about 30:1  
437 (SI Figure S4) indicating a highly regioselective dealkylation of  
438 atrazine. In addition, two other metabolites were identified as an  
439 AETOH species and an AETOxo species (see Figure 1 and SI  
440 Table S1 and Figure S4). The AETOH species was not identical

441 with the authentic standard  $\beta$ -AETOH (2-((4-chloro-6-  
442 (isopropylamino)-1,3,5-triazine-2-yl)amino)ethanol, even though  
443 it had the same mass of the molecular ion (232 m/z) and  
444 practically the same fragmentation pattern (188, 172, 146 m/z).  
445 However, it eluted at a later retention time indicating that it was  
446 either  $\alpha$ -AETOH (1-((4-chloro-6-(isopropylamino)-1,3,5-triazine-  
447 2-yl)amino)ethanol) or, possibly, a hydroxylamine (N-OH)  
448 species. An increase and subsequent decrease of concentrations  
449 was observed for AETOH and AETOxo, however, indicating that  
450 AETOH was the precursor of AETOxo and that both were  
451 therefore oxidized in the same molecular position.



454 **Figure 1.** Degradation pathways of atrazine (A) and simazine (B) with the detected metabolites formed during transformation by (1) *Rhodococcus* sp. strain  
455 NI86/21, (2) permanganate and (3) a 5,10,15,20-tetrakis(pentafluorophenyl)porphyrin iron(III) chloride complex. Products in shadow boxes were identified  
456 by comparison with authentic standards, products in thin boxes were identified by LC-MS/MS spectra. Solid arrows indicate products of  $\alpha$ -oxidation,  
457 dashed arrows indicate products of  $\beta$ -oxidation.  $\alpha$ -AETOxo (oxidation) and DEA (carbinolamine hydrolysis) are both formed from  $\alpha$ -AETOH. In addition,  
458 DEA may derive from deacylation of  $\alpha$ -AETOxo to DEA, as indicated by the arrow below the corresponding structure boxes. The same is illustrated for the  
459 simazine transformation pathway.



Cite this: DOI: 10.1039/c0xx00000x

www.rsc.org/xxxxxx

Since such a pathway is not plausible with an N-OH intermediate, the two species can be inferred to be  $\alpha$ -AETOH and  $\alpha$ -AETOxo (2-acetamido-4-chloro-6-(isopropylamino)-s-triazine). Therefore, DEA was formed by either direct decay of the carbinolamine  $\alpha$ -AETOH, or by oxidative amide cleavage of the keto product  $\alpha$ -AETOxo. In addition, neither metabolite was observed at the end of the permanganate experiment demonstrating that they were both intermediates of DEA and further confirming that they were the oxidation products of the upper pathway illustrated in Figure 1A. Permanganate oxidation therefore proved to be highly regioselective, not only with preference for the ethyl over the isopropyl group (see also SI Figure S1), but also for the  $\alpha$  over the  $\beta$  position within a given alkyl group.

*Degradation products in oxidation of simazine with  $MnO_4^-$ .* In analogy to atrazine, the  $\alpha$ -position of the ethyl group of simazine was selectively oxidized by permanganate. A more detailed description is provided in the SI.

*Atrazine degradation products in oxidation with an iron porphyrin model system (FeP).* Similar to the oxidation of atrazine by permanganate, atrazine deethylation was also highly selective with the iron porphyrin model system. The only products observed were (see Figure 1 and SI Figure S5)  $\alpha$ -AETOH (identical mass fragmentation and retention times as the product of the permanganate system) and DEA. Selective oxidation and dealkylation of atrazine by other metalloporphyrin systems were also found in studies of Rebelo<sup>78</sup> and Gotardo<sup>79</sup>.

*Atrazine degradation products with *Rhodococcus sp.* NI86/21.* Evidence was obtained for five metabolites that formed during biotic degradation of atrazine by *Rhodococcus sp.* NI86/21. The metabolites DEA, DIA and  $\beta$ -AETOH were identified by comparison to authentic reference compounds. The structures of three further metabolites were inferred from their mass fragmentation pattern as AIPOH and AETOxo. The identity of the later structure was confirmed as  $\alpha$ -AETOxo by comparison with retention times of the product from the permanganate experiment (see above). In addition, its concentration initially increased during atrazine dealkylation, but subsequently decreased again. Thus we assume that not all of the carbinolamine decays immediately to the amine but also forms the keto product which decays by oxidative amide cleavage to DEA. In contrast, AIPOH, DEA and DIA and  $\beta$ -AETOH steadily accumulated, and the later three were the most abundant products when, after 139 hours, 85% of atrazine had been transformed (SI Figure S6) This indicates that AIPOH and  $\beta$ -AETOH were not intermediates of the pathway to DEA and DIA (Figure 1). The small amounts of AIPOH must therefore have been  $\beta$ -AIPOH (2-((4-chloro-6-(ethylamino)-1,3,5-triazine-2-yl)amino)isopropanol), since  $\alpha$ -AIPOH is expected to quickly decompose to DIA. To our

knowledge AETOH was so far solely identified during abiotic transformation of atrazine with hydroxyl radicals<sup>80-82</sup> whereas AETOxo was additionally detected during catalytic conversion of atrazine in metalloporphyrin systems imitating cytochrome P450 enzymes<sup>78, 79</sup>. The detection of AIPOH is in accordance with the  $\beta$ -hydroxylated product found in the study of Nagy et al.<sup>35</sup> using the same bacterial strain. Additionally this product was also discovered during metabolism of atrazine by mammalian hepatic cytochrome P450 enzymes<sup>83</sup>.

*Contribution of concurrent degradation pathways with *Rhodococcus sp.* NI86/21.* The relative abundance of the concurrent biotransformation reactions (oxidation at the  $\alpha$ - versus  $\beta$ -position and in the ethyl versus isopropyl group) can be estimated assuming (a) that the response of the UV/VIS detector at 220 nm is similar for the different metabolites and (b) that the dealkylated products are formed exclusively from oxidation in the  $\alpha$ -position. The first assumption is supported by good molar balances of the biodegradation experiments based on the UV signal at 220 nm (crosses in the left panels of Figure S6, SI), whereas the second assumption is in accordance with our pathway analysis described above and summarized in Figure 1. Accordingly, the contribution of oxidation in the  $\alpha$ -position of the ethyl group in atrazine is given by

$$\frac{\sum ([\text{DEA}] + [\alpha\text{-AETOxo}])}{\sum [\text{all products}]} \quad (8)$$

( $\alpha$ -AETOH was not detected) whereas the contribution of oxidation in the  $\beta$ -position of the ethyl group is given as

$$\frac{[\beta\text{-AETOH}]}{\sum [\text{all products}]} \quad (9)$$

where square brackets indicate UV absorbances at 220 nm. An analogous analysis can be performed for the isopropyl group. This gives the following estimates for position-specific oxidation of atrazine:

- in the  $\alpha$ -position of the ethyl group: 35%  $\pm$  4% (SD).
- in the  $\beta$ -position of the ethyl group: 34%  $\pm$  4% (SD)
- in the  $\alpha$ -position of the isopropyl group: 17%  $\pm$  2% (SD)
- in the  $\beta$ -position of the isopropyl group: 14%  $\pm$  1% (SD).

Similarly, for simazine:

- in the  $\alpha$ -position of the ethyl group: 85%  $\pm$  1% (SD).
- in the  $\beta$ -position of the ethyl group: 15%  $\pm$  1% (SD).

These results demonstrate that (i) the preference for oxidation in the ethyl over the isopropyl group of atrazine was 2.1:1 and (ii) that oxidation in the  $\alpha$ -positions occurred to 52% in atrazine and

to 73% in simazine. After normalizing for the number of C-H bonds in each position, the preference for oxidation of a tertiary C-H bond (in  $\alpha$ -position of the isopropyl group of atrazine) over a primary C-H bond (in  $\beta$ -position of the same group) was 7.3:1. In comparison, the preference for oxidation of a secondary C-H (in  $\alpha$ -position of the ethyl group of atrazine) over a primary C-H (in  $\beta$ -position of the same group) was only 1.5:1. In contrast, it was 8.5:1 in the ethyl group of simazine. These results demonstrate that:

(i) in *Rhodococcus* sp. NI86/21 atrazine was not oxidized selectively in the  $\alpha$ -position of the side chain – as expected for SET, and observed with  $\text{MnO}_4^-$  and FeP – but instead in the  $\alpha$ - and  $\beta$ -positions, as expected for a radical reaction.

(ii) The selectivity – i.e., the reactivity of tertiary C-H bonds compared to secondary or primary C-H bonds – is reminiscent of a non-selective radical reaction (e.g., similar to an Cl radical)<sup>84</sup>. However, the inconsistent selectivities derived for the ethyl groups of atrazine and simazine demonstrate that enzyme-specific steric factors must also be important (e.g., the accessibility of C-H bonds based on the binding mode of the substrate within the enzymatic site).

**(ii) Insight from carbon, nitrogen and hydrogen isotope effects.**

*Theoretical isotope effect computations for SET or HAT in atrazine.* Table 1 summarizes the position-specific isotope effects computed for SET and HAT in atrazine, together with the compound average  $\text{AKIE}_{\text{carbon}}$  and  $\text{AKIE}_{\text{nitrogen}}$  calculated according to equation 4.

*SET versus HAT.* Theoretical density functional calculations which assumed an outer-sphere electron transfer (SET) in the initial reaction step resulted in inverse kinetic isotope effects for nitrogen – as reported in Skarpeli-Liati et al.<sup>48</sup> – and also inverse kinetic isotope effects for carbon, with an average over all positions of  $\text{AKIE}_{\text{carbon}} = 0.9965$  and  $\text{AKIE}_{\text{nitrogen}} = 0.9989$ . The inverse nature of the isotope effect can be explained by delocalization of electrons in the radical cation leading to a hybridization change and, therefore, to stiffer C-N bonds in the transition state, affecting the driving force and thereby the Marcus-theory free energy of activation<sup>48</sup>. In contrast, the scenario of hydrogen atom abstraction (HAT) at the  $\alpha$ C-atom by an active oxygen species gave kinetic isotope effects that were normal and primary for C, and normal and secondary for N, respectively. These different trends indicate that starkly contrasting isotope effect trends are expected for SET and HAT making it an expedient tool to distinguish these mechanisms.

Table 1. Theoretical and measured kinetic isotope effects for the initial step in oxidative dealkylation.

Calculated isotope effects for single electron transfer (SET) and hydrogen atom abstraction (HAT) <sup>a)</sup>								
Hydrogen atom abstraction	ethyl group ( $\alpha$ C)	ethyl group ( $\beta$ C)	isopropyl group ( $\alpha$ C)	isopropyl group ( $\beta$ C)				
	position-specific isotope effects		position-specific isotope effects		position-specific isotope effects			
	<b>Compound average</b> Carbon $\text{AKIE}_{\text{average}} = 1.0068$ Nitrogen $\text{AKIE}_{\text{average}} = 1.0016$		<b>Compound average</b> Carbon $\text{AKIE}_{\text{average}} = 1.0065$ Nitrogen $\text{AKIE}_{\text{average}} = 1.0000$		<b>Compound average</b> Carbon $\text{AKIE}_{\text{average}} = 1.0087$ Nitrogen $\text{AKIE}_{\text{average}} = 1.0024$			
Single electron transfer	<b>Measured isotope effects (Compound average)<sup>b)</sup></b>							
	position-specific isotope effects							
	<b>Compound average</b> Carbon $\text{AKIE}_{\text{average}} = 0.9965$ Nitrogen $\text{AKIE}_{\text{average}} = 0.9989$							
		substance	$\epsilon_{\text{carbon}}$ [%]	$\epsilon_{\text{nitrogen}}$ [%]	$\text{AKIE}_{\text{average/carbon}}$	$\text{AKIE}_{\text{average/nitrogen}}$ <sup>c)</sup>		
		<b>biotic oxidation</b>						
		<i>Rhodococcus</i> sp. strain NI86/21	atrazine	$4.0 \pm 0.2$	$-1.4 \pm 0.3$	$1.0040 \pm 0.0002$	$1.0014 \pm 0.0003$	$0.36 \pm 0.06$
			simazine	$4.1 \pm 0.1$	$-1.9 \pm 0.3$	$1.0041 \pm 0.0002$	$1.0019 \pm 0.0003$	$0.46 \pm 0.08$
		<b>abiotic oxidation</b>						
		KMnO <sub>4</sub>	atrazine	$4.6 \pm 0.6$	$-0.3 \pm 0.2$	$1.0046 \pm 0.0006$	$1.0003 \pm 0.0002$	$0.06 \pm 0.06$
			simazine	$4.4 \pm 0.5$	$-0.1 \pm 0.2$	$1.0044 \pm 0.0005$	$1.0001 \pm 0.0002$	$0.01 \pm 0.06$
		FeP	atrazine	$2.4 \pm 0.2$	$-1.9 \pm 0.4$	$1.0024 \pm 0.0002$	$1.0019 \pm 0.0004$	$0.88 \pm 0.70$

a) Calculated values correspond to position-specific kinetic isotope effects associated with single electron transfer, with hydrogen atom abstraction in the  $\alpha$ -position of the alkyl chain, or with hydrogen atom abstraction in the  $\beta$ -position, respectively. In contrast,  $\text{AKIE}_{\text{average}}$  are calculated as average isotope effects for carbon and nitrogen of all molecular positions.

b) Measured isotope effects are expressed as  $\epsilon_{\text{carbon}}$  and  $\epsilon_{\text{nitrogen}}$  for oxidation of atrazine and simazine by *Rhodococcus* sp. strain NI86/21, permanganate and 5,10,15,20-tetrakis(pentafluorophenyl)porphyrin iron(III) chloride (FeP).  $\text{AKIE}_{\text{average/carbon}}$  and  $\text{AKIE}_{\text{average/nitrogen}}$  are calculated according to equation 4, where uncertainties denote 95% confidence intervals.

c)  $\Lambda$  represent dual element isotope slopes of carbon and nitrogen. Uncertainties given are for 95% confidence intervals of combined data sets.



Cite this: DOI: 10.1039/c0xx00000x

www.rsc.org/xxxxxx

## ARTICLE TYPE

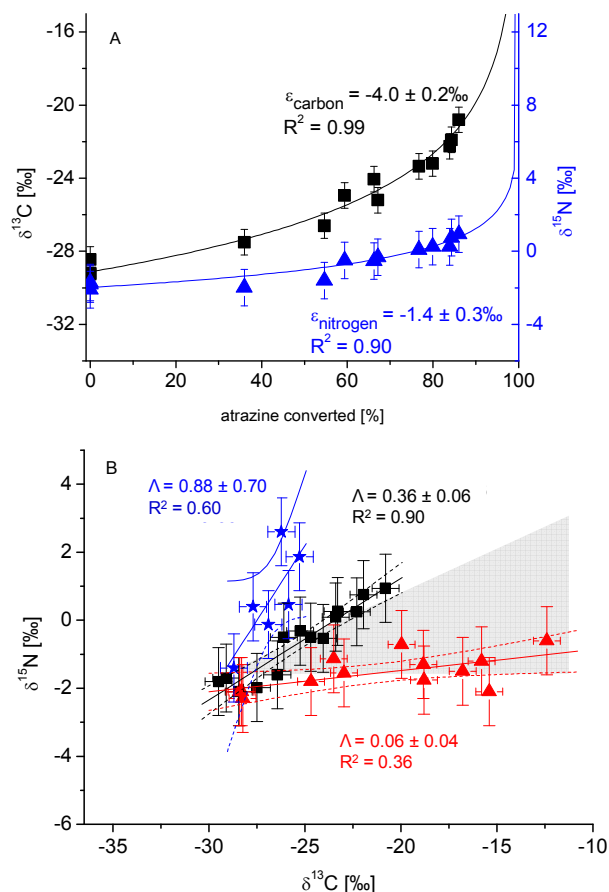


**Figure 2.** (A) Changes in carbon (black squares, left y-axis) and nitrogen (blue triangles, right y-axis) isotope values of atrazine during degradation by *Rhodococcus* sp. strain NI86/21, together with Rayleigh fits and corresponding enrichment factors  $\epsilon$ . (B) Dual isotope plots of carbon versus nitrogen for degradation of atrazine by *Rhodococcus* sp. strain NI86/21 (black squares), permanganate (red triangles) and 5,10,15,20-tetrakis(pentafluorophenyl)porphyrin iron(III) chloride (blue stars). Error bars indicate the total uncertainty of carbon ( $\pm 0.7\text{‰}$ ) and nitrogen isotope values ( $\pm 1.0\text{‰}$ ). The grey field indicates the range of slopes theoretically predicted for HAT in  $\alpha\text{C}$  and  $\beta\text{C}$  position of the alkyl group (see also SI Figure S7). Regressions are given together with 95% confidence intervals.

*Observed intermolecular isotope effects during biotic oxidation of atrazine and simazine.* Oxidation by *Rhodococcus* sp. IN86/21 led to an enrichment of  $^{13}\text{C}$  and  $^{15}\text{N}$  in atrazine and simazine (Figure 2a and Figure S8B, SI) corresponding to normal primary (= large) isotope effects for C and normal secondary (= small) isotope effects for N. No isotope fractionation was observed in sterile controls (data not shown). Both the trend of isotope effects (i.e., the normal direction) and their magnitude (i.e., primary effects for C, secondary for N) agree well with computational calculations for HAT.

This provides strong additional evidence for a HAT reaction mechanism and corroborates the conclusions drawn from product distributions above. Comparison of dual isotope plots also shows that the iron porphyrin (FeP) model gave isotope effects in the same direction (normal direction, stronger for carbon than for nitrogen) (Figure 2B, Figure S8D, SI) suggesting that also here a HAT mechanism was operative. As expected the dual element slope was steeper with FeP than in the case of *Rhodococcus* sp. IN86/21, because FeP generated products selectively in the  $\alpha$ -position and Table 1 predicts a greater ratio of  $\epsilon_{\text{nitrogen}} / \epsilon_{\text{carbon}}$  in the  $\alpha$ -position than in the  $\beta$ -position. Theoretical predictions for dual isotope slopes for HAT (grey area Figure 2b) appear to fall slightly below the experimental slopes suggesting that secondary nitrogen isotope effects may be underestimated by our calculations. Nevertheless, the qualitative agreement together with the strongly contrasting trend predicted for SET provide evidence for HAT as the prevailing mechanism in both systems.

*Observed intermolecular hydrogen isotope effects during biotic oxidation of simazine.* Competition experiments with deuterium-labelled simazine (2,4-bis(pentadeuterioethylamino)-6-chloro-1,3,5-triazine) fed to *Rhodococcus* sp. IN86/21 gave an intermolecular  $\text{KIE}_{\text{H,ethyl side chain}}$  of  $3.6 \pm 0.8$  (lumped product of primary and secondary isotope effects in the ethyl side chain of the triazine, SI, Figure S9). While clearly of primary nature, the value is also indicative of mixed rate-limiting behaviour, as expected in enzymatic reactions when commitment to catalysis is not negligible<sup>62</sup>. Evidence for commitment of catalysis in *Rhodococcus* sp. strain NI86/21 is given by a comparison of calculated and observed  $\epsilon_{\text{carbon}}$  ( $\epsilon_{\text{carbon, calculated}} > \epsilon_{\text{carbon, observed}}$ , see Table 1) which indicate that the intrinsic  $\text{KIE}_{\text{H}}$  is likely greater than 3.6. Such a pronounced hydrogen isotope effect provides further support for a HAT in *Rhodococcus* sp. strain NI86/21 confirming the results from product distribution,  $\text{AKIE}_{\text{carbon}}$  and  $\text{AKIE}_{\text{nitrogen}}$ .

As alternative to HAT, a stepwise proton and electron transfer, or a proton-coupled electron transfer (PCET), has recently brought forward as mechanistic possibility in several cases<sup>85-87</sup> raising the question whether PCET may alternatively explain the isotope effects of our study. A closer examination, however, shows that this scenario is most unlikely: The transition state would correspond to a radical ylide (a carbanion adjacent to an amine radical cation), which would formally be an excited electronic state of the product system and hence not relevant to the path on the ground electronic state potential energy surface. Thus, we conclude that this mechanistic possibility may be excluded for energetic reasons.

*Observed intermolecular isotope effects during oxidation of atrazine and simazine with permanganate.*

Observed isotope effects are different for abiotic oxidation by

$\text{MnO}_4^-$ . Despite pronounced carbon isotope effects of  $\text{AKIE}_{\text{average,carbon}}$  of  $1.0046 \pm 0.0006$  (atrazine) and  $1.0044 \pm 0.0005$  (simazine) (Figure S8B/C), no significant N isotope fractionation was observed in both compounds corresponding to a slope of zero in Figure 2. This trend would be consistent with HAT in the  $\beta$ -position (Table 1), but not with HAT oxidation products in the  $\alpha$ -position, as observed for permanganate. Therefore, the highly selective reaction at the  $\alpha$ -C atom must be attributable to a different mechanism. Computations are provided in the Supporting Information for (i) HAT with permanganate, as well as (ii) mimicking a hydride transfer through a dissociative mechanism so that a positive charge develops at the carbon center (Supporting Information Figure S3, Table S11-13). For the HAT mechanism with permanganate, the nature of the transition states (Figure S9) and the values of isotope effects are essentially identical to those for HAT computed in Table 1 (normal carbon and normal nitrogen isotope effects). For the  $\text{S}_{\text{N}}1$ -like hydride transfer, computations yielded normal carbon, but inverse nitrogen isotope effects (SI, Figure S3, S9, Table S17-19). The inverse nitrogen isotope effects are consistent with previous observations and calculations for N-containing compounds by Fitzpatrick *et al.*<sup>46,47</sup>

Since neither result agrees with our experimental data for permanganate, alternative explanations are warranted. One explanation is that HAT and dissociative hydride transfer occurred simultaneously with permanganate. The normal carbon isotope effects of each reaction would reinforce each other, whereas the normal and inverse nitrogen isotope effects would cancel out. Alternatively – and more likely – our results may indeed be indicative of a hydride transfer according to an associative mechanism as brought forward by Gardner and Mayer<sup>40</sup>. In contrast to the dissociative hydride transfer, a hydroxide displaces the hydride when it is being abstracted by the oxygen of Mn-O. Small kinetic isotope effects in  $\alpha$ -position are not unusual in  $\text{S}_{\text{N}}2$  reactions, because two counter effects are at work: (a) a small normal isotope effect caused by stabilization of a transient charge at the associative reaction centre and (b) a small inverse effect due to bending vibrations of higher energy which are caused by the more cramped coordination sphere (5 nominal substituents) in the transition state of an associative reaction.

## CONCLUSION

A combined approach using isotope effect analysis and product distribution measurements provides compelling evidence for hydrogen atom transfer (HAT) as the initial step in the oxidative dealkylation of triazines with *Rhodococcus* sp. strain NI86/21. Since biodegradation by this organism is well-established to involve a cytochrome P450 monooxygenase system, this result is important for understanding the reaction chemistry of P450 enzymes. Our results demonstrate that the HAT mechanism, which is well-established for selective oxidation of hydrocarbons by P450, also extends to N-dealkylation. This highlights a mechanistic scheme in which selectivity is likely governed by radical reactivity, and by the architecture of the enzymatic site.

In addition, the combined approach using the two mechanistic probes described here (carbon, nitrogen, hydrogen isotope effects / product distribution) holds promise for identifying the mechanisms of other relevant transformation reactions. Of particular note, the contrasting nature of predicted KIEs for HAT vs. single electron transfer (SET) mechanisms indicates that isotope effect studies may be an expedient tool to identify the occurrence of HAT or SET in future studies. This was recently also substantiated by studies of Skarpeli-Liati *et al.*<sup>48,88</sup> on oxidative transformations of substituted aromatic N-dialkyl anilines with manganese oxide and horseradish peroxidase as oxidants. Experimentally observed patterns of C, N and H isotope effects agree with our results in a remarkable way. With 4-chloro dimethylaniline the corresponding monoalkyl aniline was produced, indicative of dealkylation. Small normal N-isotope effects, as well as large normal C (up to 1.019) and H (up to 3.1) isotope effects were observed, in strong agreement with the isotope effects measured in our study for a HAT mechanism. N-dialkylamines with less electronegative substituents, in contrast, gave mainly radical coupling products rather than N-dealkylation, indicative of a SET mechanism. This pathway was associated with significant inverse N (up to 0.991) isotope effects, consistent with our calculations for SET. Although Skarpeli-Liati *et al.* did not exclude the possibility of a universal SET mechanism, our results rather support their alternative explanation: that a transition from HAT to SET mechanism took place. Therefore, the study by Skarpeli-Liati *et al.* does not only provide additional experimental support for the mechanistic conclusions of our study. It also gives an exciting glimpse that the mechanism may change within the same experimental system depending on the redox potential of organic target compounds. The same conclusion has very recently been brought forward by Morimoto *et al.* for oxidation of benzyl alcohol derivatives<sup>89</sup>.

## ACKNOWLEDGMENTS

This work was conducted in a Helmholtz Young Investigator Group supported by funding of the Helmholtz Initiative and Networking Fund and the priority program SPP 1315 of the German National Science Foundation. We thank Michael Sander (ETH Zürich) for preliminary experiments setting a lower limit to the oxidation potential of atrazine, and Frederick von Netzer for helpful discussions. ADD thanks the Polish-American Fulbright Commission for financial support (the Senior Research Grant (2011-2012)). Access to supercomputing facilities at the University of Minnesota (Minnesota Supercomputing Institute), and the Computer Center of the Lodz University of Technology (BlueOcean cluster) is gratefully acknowledged. IG acknowledges the European Union under the 7th Framework Programme (project acronym CSI: ENVIRONMENT, contract number PITN-GA-2010-264329) for her PhD stay at TUL. PJA thanks the NSF (0618784) for funding. ADS thanks the Peach Foundation for an undergraduate research fellowship.

## Notes and references

<sup>a</sup>Institute of Groundwater Ecology, Helmholtz Zentrum München, Ingolstädter Landstraße 1, 85764 Neuherberg, Germany.

<sup>b</sup>Institute of Applied Radiation Chemistry, Faculty of Chemistry, Lodz

<sup>c</sup>University of Technology, Zeromskiego 116, 90-924 Lodz, Poland.

<sup>d</sup>Department of Chemistry, Seattle University, 901 12th Avenue, Seattle, WA 98122, USA.

<sup>e</sup>Department of Chemistry and Supercomputing Institute, University of Minnesota, 207 Pleasant St. SE, Minneapolis, Minnesota 55455, USA.

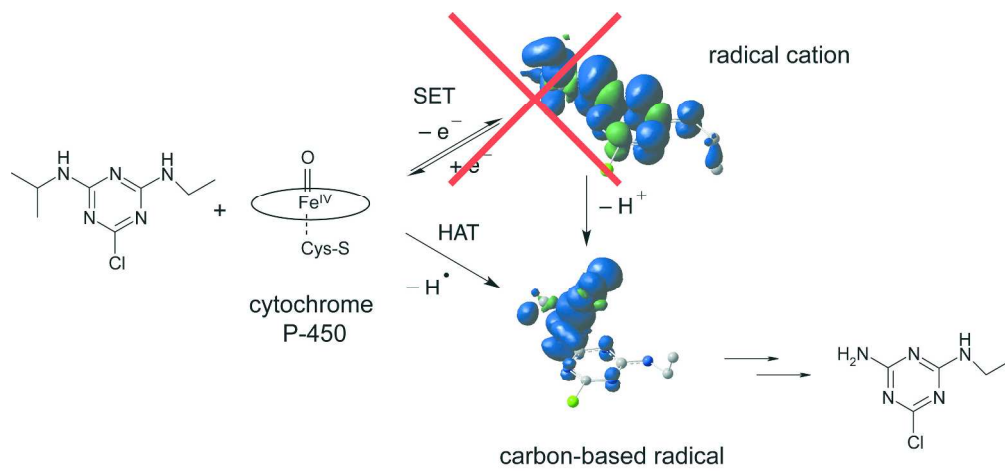
ABBREVIATIONS: DEA, desethylatrazine; DIP, desisopropylatrazine, SET, single electron transfer; HAT, hydrogen atom abstraction; FeP, metalloporphyrine system 5,10,15,20-tetrakis(pentafluorophenyl)porphyrin-iron(III)-chloride; SI, supporting information; KIE, kinetic isotope effect, GC-IRMS, gas chromatography - isotope mass spectrometry; LC-MS/MS, liquid chromatography mass spectrometry/mass spectrometry; HPLC-UV/VIS, high performance liquid chromatography ultraviolet-visible spectrophotometry;  $\epsilon$ , isotope enrichment factor.

† Electronic Supplementary Information (ESI) available: More detailed description about the experimental setup, synthesis of standard, analyses and computation of carbon nitrogen and hydrogen isotope effects. Presentation of degradation products in biotic and abiotic reference systems. Complementary presentation of theoretical and observed isotope effects associated to oxidative degradation of triazines. See DOI: 10.1039/b000000x/

1. F. P. Guengerich, *J. Biochem. Mol. Toxicol.*, 2007, **21**, 163-168.
2. P. R. Ortiz de Montellano, ed., *Cytochrome P450: Structure, Mechanism and Biochemistry*, Kluwer Academic/Plenum, New York, 2005.
3. P. Anzenbacher and E. Anzenbacherová, *Cell. Mol. Life. Sci.*, 2001, **58**, 737-747.
4. L.-L. Wong, *Curr. Opin. Chem. Biol.*, 1998, **2**, 263-268.
5. M. W. Peters, P. Meinhold, A. Glieder and F. H. Arnold, *J. Am. Chem. Soc.*, 2003, **125**, 13442-13450.
6. A. Siriphongphaew, P. Pisuong, J. Wongkongkatep, P. Inprakhon, A. Vangnai, K. Honda, H. Ohtake, J. Kato, J. Ogawa, S. Shimizu, V. Urlacher, R. Schmid and T. Pongtharangkul, *Appl. Microbiol. Biot.*, 2012, **95**, 357-367.
7. V. B. Urlacher and M. Girhard, *Trends Biotechnol.*, 2012, **30**, 26-36.
8. S. G. Sligar, *Science*, 2010, **330**, 924-925.
9. J. Rittle and M. T. Green, *Science*, 2010, **330**, 933-937.
10. X.-L. Sun, X.-R. Huang, J.-L. Li, R.-P. Huo and C.-C. Sun, *Journal of Phys. Chem. A*, 2012, **116**, 1475-1485.
11. F. P. Guengerich and T. L. MacDonald, *FASEB J.*, 1990, **4**, 2453-2459.
12. P. R. Ortiz de Montellano, *Chem. Rev.*, 2009, **110**, 932-948.
13. M. Stiborova, H. H. Schmeiser and E. Frei, *Phytochemistry*, 2000, **54**, 353-362.
14. F. P. Guengerich, C. H. Yun and T. L. MacDonald, *J. Biol. Chem.*, 1996, **271**, 27321-27329.
15. T. Robineau, Y. Batard, S. Nedelkina, F. Cabello-Hurtado, M. LeRet, O. Sorokine, L. Didierjean and D. Werck-Reichhart, *Plant Physiol.*, 1998, **118**, 1049-1056.
16. S. Shaik, S. Cohen, Y. Wang, H. Chen, D. Kumar and W. Thiel, *Chem. Rev.*, 2009, **110**, 949-1017.
17. S. B. Karki, J. P. Dinnocenzo, J. P. Jones and K. R. Korzekwa, *J. Am. Chem. Soc.*, 1995, **117**, 3657-3664.
18. M. Sono, M. P. Roach, E. D. Coulter and J. H. Dawson, *Chem. Rev.*, 1996, **96**, 2841-2888.
19. F. P. Guengerich, *Chem. Res. Toxicol.*, 2001, **14**, 611-650.
20. G. T. Miwa, J. S. Walsh, G. L. Kedderis and P. F. Hollenberg, *J. Biol. Chem.*, 1983, **258**, 14445-14449.
21. L. R. Hall and R. P. Hanzlik, *Xenobiotica*, 1991, **21**, 1127-1138.
22. Y. Wang, D. Kumar, C. Yang, K. Han and S. Shaik, *J. Phys. Chem. B*, 2007, **111**, 7700-7710.
23. J. P. Dinnocenzo, S. B. Karki and J. P. Jones, *J. Am. Chem. Soc.*, 1993, **115**, 7111-7116.
24. M. N. Bhakta and K. Wimalasena, *J. Am. Chem. Soc.*, 2002, **124**, 1844-1845.
25. C. M. Brown, B. Reisfeld and A. N. Mayeno, *Drug Metab. Rev.*, 2008, **40**, 1-100.
26. L. T. Burka, F. P. Guengerich, R. J. Willard and T. L. Macdonald, *J. Am. Chem. Soc.*, 1985, **107**, 2549-2551.
27. G. Galliani, M. Nali, B. Rindone, S. Tollari, M. Rocchetti and M. Salmona, *Xenobiotica*, 1986, **16**, 511-517.
28. F. P. Guengerich, *J LABELLED COMPD RAD*, 2013, **56**, 428-431.
29. L. R. Hall and R. P. Hanzlik, *J. Biol. Chem.*, 1990, **265**, 12349-12355.
30. J. I. Manchester, J. P. Dinnocenzo, L. A. Higgins and J. P. Jones, *J. Am. Chem. Soc.*, 1997, **119**, 5069-5070.
31. A. Kohen, in *Isotope Effects in Chemistry and Biology*, eds. A. Kohen and H.-H. Limbach, CRC Press, Bac Raton, London, New York, 2006, ch. 28, pp. 743-764.
32. T. J. Carlson, J. P. Jones, L. Peterson, N. Castagnoli, K. R. Iyer and W. F. Trager, *Drug. Metab. Dispos.*, 1995, **23**, 749-756.
33. P. Ortiz de Montellano and J. J. De Voss, *Nat Prod Rep.*, 2002, **19**, 477-493.
34. B. Meunier, S. P. de Visser and S. Shaik, *Chem. Rev.*, 2004, **104**, 3947-3980.
35. I. Nagy, F. Compernelle, K. Ghys, J. Vanderleyden and R. De Mot, *Appl. Environ. Microbiol.*, 1995, **61**, 2056-2060.
36. I. Nagy, G. Schoofs, F. Compernelle, P. Proost, J. Vanderleyden and R. Mot de, *J. Bacteriol.*, 1995, **177**, 676-687.
37. M. C. Feiters, A. E. Rowan and R. J. M. Nolte, *Chem. Soc. Rev.*, 2000, **29**, 375-384.
38. M. M. Wei and R. Steward, *J. Am. Chem. Soc.*, 1966, **88**, 1974-1979.
39. M. Elsner, J. McKelvie, G. LacrampeCouloume and B. SherwoodLollar, *Environ. Sci. Technol.*, 2007, **41**, 5693-5700.
40. K. A. Gardner and J. M. Mayer, *Science*, 1995, **269**, 1849-1851.
41. V. L. Lobachev and E. S. Rudakov, *Kinet. Catal.*, 1994, **35**, 203-210.
42. P. Adamczyk, A. Dybala-Defratyka and P. Paneth, *Environ. Sci. Technol.*, 2011, **45**, 3006-3011.
43. Y.-R. Fang, Y. Q. Gao, P. Ryberg, J. Eriksson, M. Kołodziejska-Huben, A. Dybala-Defratyka, S. Madhavan, R. Danielsson, P. Paneth, O. Matsson and K. C. Westaway, *Chem. Eur. J.*, 2003, **9**, 2696-2709.
44. R. J. Robins, R. Molini, E. R. Kwiecie, P. Paneth, J. Lebreton, T. Bartholomeusz, A. D. Roscher, B. ger, A.-C. Meier and F. Mesnard, *Phytochem. Rev.*, 2007, **6**, 51-63.
45. R. Molinié, R. A. Kwiecien, P. Paneth, W. Hatton, J. Lebreton and R. J. Robins, *Arch. Biochem. Biophys.*, 2007, **458**, 175-183.
46. E. C. Ralph, J. S. Hirschi, M. A. Anderson, W. W. Cleland, D. A. Singleton and P. F. Fitzpatrick, *Biochem.*, 2007, **46**, 7655-7664.
47. P. F. Fitzpatrick, *J. of Label. Compd. Radiopharm.*, 2007, **50**, 1016-1025.
48. M. Skarpeli-Liati, M. Jiskra, A. Turgeon, A. N. Garr, W. A. Arnold, C. J. Cramer, R. P. Schwarzenbach and T. B. Hofstetter, *Environ. Sci. Technol.*, 2011, **45**, 5596-5604.
49. J. Sinha, S. J. Reyes and J. P. Gallivan, *Nat Chem Biol*, **6**, 464-470.
50. W. C. Still, M. Kahn and A. Mitra, *J. Org. Chem.*, 1978, **43**, 2923-2925.
51. S. Reinnicke, D. Juchelka, S. Steinbeiss, A. H. Meyer, A. Hilker and M. Elsner, *Rapid. Commun. Mass. Sp.*, 2012, **26**, 1053-1060.
52. A. E. Hartenbach, T. B. Hofstetter, P. R. Tentscher, S. Canonica, M. Berg and R. P. Schwarzenbach, *Environ. Sci. Technol.*, 2008, **42**, 7751-7756.

53. A. H. Meyer, H. Penning, H. Lowag and M. Elsner, *Environ. Sci. Technol.*, 2008, **42**, 7757-7763.
54. M. Elsner, M. A. Jochmann, T. B. Hofstetter, D. Hunkeler, A. Bernstein, T. C. Schmidt and A. Schimmelmann, *Anal. Bioanal. Chem.*, 2012, **403**, 2471-2491.
55. D. Hunkeler, R. U. Meckenstock and H. H. Richnow, *Appl Environ. Microbiol.*, 2002, **68**, 5205-5207.
56. M. Elsner, *J. Environ. Monit.*, 2010, **12**, 2005-2031.
57. A. Fischer, I. Herklotz, S. Herrmann, M. Thullner, S. A. B. Weelink, A. J. M. Stams, M. Schlömann, H.-H. Richnow and C. Vogt, *Environ. Sci. Technol.*, 2008, **42**, 4356-4363.
58. H. Penning, S. R. Sorensen, A. H. Meyer, J. Aamand and M. Elsner, *Environ. Sci. Technol.*, 2010, **44**, 2372-2378.
59. T. B. Hofstetter, J. C. Spain, S. F. Nishino, J. Bolotin and R. P. Schwarzenbach, *Environ. Sci. Technol.*, 2008, **42**, 4764-4770.
60. A. H. Meyer, H. Penning and M. Elsner, *Environ. Sci. Technol.*, 2009, **43**, 8079-8085.
61. P. Paneth, *J. Mol. Struct.*, 1994, **321**, 35-44.
62. D. B. Northrop, *Annu. Rev. Biochem.*, 1981, **50**, 103-131.
63. Y. Zhao and D. G. Truhlar, *Accounts of Chem. Res.*, 2008, **41**, 157-167.
64. Y. Zhao and D. G. Truhlar, *Theor. Chem. Acc.*, 2008, **120**, 215-241.
65. P. C. Hariharan and J. A. Pople, *Theor. Chem. Acc.*, 1973, **28**, 213-222.
66. M. M. Francl, W. J. Pietro, W. J. Hehre, J. S. Binkley, M. S. Gordon, D. J. DeFrees and J. A. Pople, *J. Chem. Phys.*, 1982, **77**.
67. A. V. Marenich, C. J. Cramer and D. G. Truhlar, *J. Phys. Chem. B*, 2009, **113**, 6378-6396.
68. M. J. Frisch, *Gaussian, Inc.: Wallingford, CT.*, 2009.
69. A. Kavner, F. Bonet, A. Shahar, J. Simon and E. Young, *Geochim. Cosmochim. Ac.*, 2005, **69**, 2971-2979.
70. A. D. McLean and G. S. Chandler, *J. Chem. Phys.*, 1980, **72**.
71. R. Krishnan, J. S. Binkley, R. Seeger and J. A. Pople, *J. Chem. Phys.*, 1980, **72**, 650-655.
72. E. Buhks, M. Bixon, J. Jortner and G. Navon, *The Journal of Physical Chemistry*, 1981, **85**, 3759-3762.
73. E. Buhks, M. Bixon and J. Jortner, *The Journal of Physical Chemistry*, 1981, **85**, 3763-3766.
74. J. P. Roth, R. Wincek, G. Nodet, D. E. Edmondson, W. S. McIntire and J. P. Klinman, *Journal of the American Chemical Society*, 2004, **126**, 15120-15131.
75. J. Bigeleisen, *J. Chem. Phys.*, 1949, **17**, 675-679.
76. V. Anisimov and P. Paneth, *J. Math. Chem.*, 1999, **26**.
77. R. T. Skodje, D. G. Truhlar and B. C. Garrett, *J. Phys. Org. Chem.*, 1981, **85**, 3019-3023.
78. S. L. H. Rebelo, M. M. Pereira, P. V. Monsanto and H. D. Burrows, *J. Mol. Catal. A-Chem.*, 2009, **297**, 35-43.
79. M. A. F. Gotardo, L. A. B. De Moraes and M. D. Assis, *J. Agric. Food Chem.*, 2006, **54**, 1011-10018.
80. M. S. Arnold, R. E. Talaat, W. J. Hickey and R. F. Harris, *J. Mass. Spec.*, 1995, **30**, 452-460.
81. K. H. Chan and W. Chu, *J. Hazard. Mater.*, 2005, **118**, 227-237.
82. T. A. McMurray, P. S. M. Dunlop and J. A. Byrne, *J. Photoch. Photobio. A*, 2006, **182**, 43-51.
83. N. Hanioka, H. Jinno, K. Kitazawa, T. Tanaka-Kagawa, T. Nishimura, M. Ando and K. Ogawa, *Chem-Biol Interact.*, 1998, **116**, 181-198.
84. M. B. Smith and J. March, eds., *Advanced Organic Chemistry, Reactions, Mechanisms, and Structure*, Wiley-Interscience, New York, 2001.
85. S. Hammes-Schiffer and A. A. Stuchebrukhov, *Chem. Rev.*, 2010, **110**, 6939-6960.
86. D. Usharani, D. C. Lacy, A. S. Borovik and S. Shaik, *J. Am. Chem. Soc.*, 2013, **135**, 17090-17104.
87. J. M. Mayer, *Annu. Rev. Phys. Chem.*, 2004, **55**, 363-390.
88. M. Skarpetli-Liati, S. G. Pati, J. Bolotin, S. N. Eustis and T. B. Hofstetter, *Environ. Sci. Technol.*, 2012, **46**, 7189-7198.
89. Y. Morimoto, J. Park, T. Suenobu, Y.-M. Lee, W. Nam and S. Fukuzumi, *Inorg. Chem.*, 2012, **51**, 10025-10036.

Isotope effects and position-specificity of hydroxylation pinpoint hydrogen atom transfer (HAT) as prevailing mechanism in P-450 catalyzed N-dealkylation of atrazine



263x121mm (300 x 300 DPI)